6-Oct-2018: Revised Manuscript for *FUEL* with Reference number *JFUE-D-18-02389R1*

Title: Viscosity of Oxygenated Fuel: A Model Based on Eyring's Absolute Rate Theory

Authors: Chenyang Zhu; Feng Yang; Xiangyang Liu; Waheed Afzal; Maogang He

Abstract

A viscosity model was proposed for oxygenated fuel components; it was based on Eyring's absolute rate theory and a cubic equation of state Soave-Redlich-Kwong. The viscosity was associated with flow energy which could be divided into the activation energy and the vacancy-formation energy, and then a reference state for simplifying the calculation process was introduced in the present model. This work also reported a viscosity database at temperatures from 243.15 K to 413.15 K and pressures up to 200 MPa for 31 oxygenated fuel components containing alcohols, esters and ethers in order to verify the proposed model. The average absolute relative deviations between calculated and experimental data were lower than 2.37%. Furthermore, the free-volume model, which has a similar consideration of flow energy with this work, was chosen to further investigate the performance of the present model, and in general, the present model showed a better accuracy than the free-volume model. Finally, it was shown that the proposed model could be extended to the mixtures successfully.

Key words

Viscosity; Eyring's absolute rate theory; Flow energy; Oxygenated fuel; Free-volume model

1. Introduction

Nowadays, with the increasing attentions on environmental protection, many researches related to new environment-friendly technologies and substances have been carried out, such as organic Rankine cycle [1], absorption refrigeration [2], concentrated solar power syngas production [3],

supercritical water gasification [4], ionic liquid [5], new refrigerant [6] and especially, oxygenated fuel [7]. The oxygenated fuel compounds are oxygen-containing hydrocarbons which are either naturally presented in fuels or used as additives to improve certain properties of interest. For example, in diesel, oxygenated hydrocarbons can reduce the pollutant emissions and improve the combustion efficiency [8]. Furthermore, the addition of oxygenated fuels will affect thermophysical properties of diesel. So the study on thermophysical and transport properties of oxygenated fuels is required for a better understanding and improvement in engines [9], which include heat capacity [10], critical properties [11] and speed of sound [12], etc. Viscosity has a significant impact on the spray characteristics and combustion of the fuel [13]. For decades, the experimental viscosity of oxygenated compounds has been widely reported [14-33] often with significant scatter. In addition to the provision of accurate data, a rigid theoretical model for the viscosity of oxygenated fuels is required to further our knowledge and assist applications.

Many efforts have been made to build a sound theory for calculation of the fluid-phase viscosity, but most of them are useful to describe the viscosities at atmospheric pressure and are empirical in nature. For examples, viscosity models include those based on the group contribution method [34, 35], the quantitative structure-property relationship method [36, 37], Lohrenz-Bray-Clark model [38] and Yarranton-Satyro model [39, 40]. Besides these, there are a few viscosity models which are applicable to a wide range of temperatures and pressures with strong physical backgrounds. Using the hard-sphere theory, Assael et al. [41] presented a method (hard-sphere model) to predict the transport properties including viscosity, self-diffusion and thermal conductivity of *n*-alkanes. A proportionality factor representing the roughness and the degree of non-sphericity of the molecule was introduced, and universal curves were found for the reduced transport properties as a function

of the reduced volume. After showing a good agreement between experimental data and calculations for the viscosity of *n*-alkanes, Assael et al. extended their model to other families of substances (such as *n*-alcohols [42], aromatic hydrocarbons [43] and refrigerants [44], etc.). Quinones-Cisneros et al. [45] presented a friction theory model for the viscosity of both gases and liquids, which is based on friction concepts of classical mechanics and the van der Waals theory of fluids. The unique idea of this theory is to consider the viscosity as a mechanical instead of a transport property. An earlier version of the friction theory model was proposed for alcohols [46], and a one-parameter [47] as well as a general [48] versions were also developed leading to their wider applications. Allal et al. [49] proposed, on the other hand, a quite simple model for viscosity, which is usually called free-volume model. The free-volume model is based on free-volume concept and the diffusion models of molecules, and it only involves three parameters for each fluid. Then the free-volume model shows an excellent performance for various fluids in both gas and liquid phases [50] as well as their mixtures [51].

Adopting the conception of absolute rate theory, Kincaid and his co-workers [52] proposed a prediction method for the viscosity of saturated liquids, which described the relation of the activation energy and dynamic viscosity of fluid. Then, many modified versions focused on effectively calculating the activation energy were presented. By correlating the activation volume with temperature and pressure directly, Xuan et al. [53] developed a quite simple viscosity model. The performance of their model was verified by 23 organic liquids with the average absolute relative deviation of 0.76%. But for each temperature, their model required one set of parameters obtained from experimental data. Martins et al. [54] proposed a viscosity model suitable to elevated pressure conditions. The basic assumption of their model is that the difference of the

activation energy is equal to the difference of the Helmholtz free energy. The high accuracies of this model combined with different EOSs were observed, while it has the same drawback with Xuan's model. Lei et al. [55] hypothesized a proportional relationship between free energy and vaporization energy, and then presented a semi-empirical model for saturated liquid. On this basis, Macías-Salinas et al. [56] proposed a correlation for viscosities at the pressures above the saturation points with 5 parameters. Nevertheless, in Macías-Salinas's model, the pressure effect on the vacancy-formation energy was ignored. It should be noted that all the hypotheses about the free energy are empirical, which will cause the additional deviations in viscosity calculation inevitably. In addition, the introduction of vaporization energy will also complicate the computing processes of the model, which is inconvenient for its practical applications. So, according to the discussions above, we can conclude that, as a promising theory for viscosity, there is no practical model applied to viscosity of liquids using Eyring's absolute rate theory, which is a rather regrettable absence for viscosity study.

Recently, Meng et al. [57] evaluated the performances of three aforementioned semi-empirical models (hard-sphere, friction-theory and free-volume models) and three empirical models for the viscosity of 9 oxygenated fuels, in which the hard-sphere and the free-volume models were recommended. However, the absolute rate theory model, one of the most widely used models for viscosity, is not tested in [57]. Therefore, this work aims to develop a simple but accurate viscosity model based on Eyring's absolute rate theory, applicable to a wide temperature and pressure range. Then, a database of the viscosities (of 31 oxygenated fuel components) was tabulated and used to verify our model. Finally, the feasibility of the model for mixtures is also examined.

The fundamental idea of the present model is to assume that the flow energy is a combination of

free energy and vacancy-formation energy. Then, a pressure term is included to relate the vacancy-formation energy. At last, to eliminate the undetermined free energy term, a reference state is introduced. Being tested by 31 oxygenated fuels and 4 mixtures, the present model for viscosity shows an excellent agreement with the experiment.

2. Viscosity model

As the liquid is assumed to be a quasi-crystal structure in Eyring's theory, each molecule can be considered as being restricted to a cell constructed by the neighboring molecules [58]. Therefore, the flow of liquid can be expressed as following process:

$$\mathrm{A} \Leftrightarrow \mathrm{X} \rightarrow \mathrm{B} \tag{1}$$

which means, to overcome the barrier energy which the molecule must cross to diffuse, the molecule "A" should obtain the activation energy and becomes activated molecule "X". Then the activated molecule will jump into a new position, vacancy "B". Lei et al. [55] considered that the molecule "A" and activated molecule "X" were in thermodynamic equilibrium, and the correlation between the equilibrium constant and the activation energy satisfied the Arrhenius-type equation. Then the following viscosity model was presented

$$\eta = \frac{RT}{\gamma V} \exp\left(\frac{\alpha \Delta G^*}{RT} \right) \exp\left(\frac{pV}{RT} \right) \tag{2}$$

where η is dynamic viscosity, γ is the frequency of the activated molecule "X" jumping into the vacancy "B", which is only related to the substance, R is the gas constant, T is absolute temperature, V is molar volume, p is pressure, α is adjustable parameter. In Eq. (2), it is notable that the flow energy is divided into two parts: the molar energy of activation ΔG^* and the energy of vacancy-formation pV.

The activation energy shall be acquired by a molecule to squeeze past its neighbors into the new

111 equilibrium position. In general view, the bonds broken in the flow process are the same to the
112 bonds broken in the process of vaporization. So the following function can be given easily

113 $$\Delta G^{*} = f\left(\Delta U_{\mathrm{vap}}\right) \tag{3}$$

114 where ΔU_{vap} is the internal energy of vaporization, f is the function symbol. The specific form of
115 $f(\Delta U_{\mathrm{vap}})$ in Eq. (3) has been discussed by several researchers [52, 55, 56]. For instance, Kincaid et
116 al. [52] thought that ΔG^{*} was proportional to the internal energy of vaporization, and gave the
117 proportionality coefficient to be (1/2.45). Lei et al. [55] also assumed a linear relationship between
118 ΔG^{*} and U_{vap}, while the proportionality coefficient was considered as an adjustable parameter.
119 Macías-Salinas et al. [56] adopted an exponential form between ΔG^{*} and U_{vap}, and two adjustable
120 parameters were required. However, these expressions of ΔG^{*} are empirical and may introduce the
121 error from calculation of vaporization energy. Therefore, the exact form of ΔG^{*} will not be
122 determined in this work. Then, substituting Eq. (3) into Eq. (2) yields

123 $$\eta_{\mathrm{l}}^{\mathrm{s}} = \frac{RT}{\gamma V_{\mathrm{l}}^{\mathrm{s}}} \exp\left[\frac{\alpha f\left(\Delta U_{\mathrm{vap}}\right) + p^{\mathrm{s}} V_{\mathrm{l}}^{\mathrm{s}}}{RT}\right] \tag{4}$$

124 in which the subscript l and the superscript s represent liquid and saturated conditions, respectively.
125 Eq. (4) is a viscosity model applied to saturated liquid, and to extend it to the compressed liquid,
126 Macías-Salinas et al. [56] propose an expression which is similar to the model for liquid mixtures

127 $$\ln\left[\frac{\eta_{\mathrm{l}} V_{\mathrm{l}}}{\left(\eta_{\mathrm{l}} V_{\mathrm{l}}\right)^{\mathrm{s}}}\right] = \frac{\Delta G^{*,p}}{RT} \tag{5}$$

128 where $\Delta G^{*,p}$ is activation energy required for compressing the saturated liquid to a higher pressure
129 p along the isothermal curve. As it has been mentioned above, the flow energy consists of
130 activation and vacancy-formation energy, whereas the additional energy which is caused by
131 forming vacancy against the increase of pressure is not considered in Eq. (5). So a vacancy term

will be introduced to modify the flow energy at elevated pressure

$$\ln\left[\frac{\eta_l V_l}{\left(\eta_l V_l\right)^s}\right]=\frac{\Delta G^{*,p}+a\left(pV_l-p^sV_l^s\right)}{RT} \tag{6}$$

where a is the parameter which can be collected as the quadratic function of reduced temperature

$$a=a_1+a_2/T_r^2 \tag{7}$$

Combining Eqs. (4, 6 and 7) and hypothesizing the effect of pressure on activation energy can be neglected, one will get

$$\eta_l=\frac{RT}{\gamma V_l}\exp\left[\frac{\alpha f\left(\Delta U_{vap}\right)}{RT}+Z_l^s+\left(a_1+a_2/T_r^2\right)\left(Z_l-Z_l^s\right)\right] \tag{8}$$

where Z is compressibility factor, γ, α, a_1 and a_2 are temperature and pressure independent parameters. As the specific form of $f(\Delta U_{vap})$ will not be determined in this work, the effort to eliminate it should be implemented. To this end, a reference state under the pressure p^0 is substituted into Eq. (8)

$$\eta_l^0=\frac{RT}{\gamma V_l^0}\exp\left[\frac{\alpha f\left(\Delta U_{vap}\right)}{RT}+Z_l^s+\left(a_1+a_2/T_r^2\right)\left(Z_l^0-Z_l^s\right)\right] \tag{9}$$

where the superscript 0 means at the reference state. Taking the ratio η_l/η_l^0 from Eqs. (8 and 9) leads to

$$\eta_l=\eta_l^0\frac{pZ_l^0}{p^0Z_l}\exp\left[\left(a_1+a_2/T_r^2\right)\left(Z_l-Z_l^0\right)\right] \tag{10}$$

In our previous work [59], the atmospheric pressure was chosen to be the reference state, and the η_l^0 was correlated by Vogel equation. However, to guarantee the reference state could be in the liquid phase at all temperatures selected in this work, we consider the critical pressure p_c as the reference pressure p^0. The viscosities of methanol (MeOH), dimethyl carbonate (DMC) and dimethoxymethane (DMM) at reduced pressure p_r=1 are plotted in Fig. 1. It shows that the natural

logarithm of viscosity at critical pressure depends linearly on the reciprocal of reduced temperature, so the reference viscosity still can be obtained by the Vogel equation [60]

$$\ln \eta_{\mathrm{l}}^{\mathrm{c}} = b + \frac{c}{d + T_{\mathrm{r}}} \tag{11}$$

where $\eta_{\mathrm{l}}^{\mathrm{c}}$ is the viscosity at critical pressure, b, c and d are parameters with values listed in Table S1. The results of Eq. (11) for the $\eta_{\mathrm{l}}^{\mathrm{c}}$ of MeOH, DMC and DMM are shown in Fig. 1, which reveal that the calculated values are in good agreement with the experimental data.

Combining Eqs. (10 and 11), the final model for calculating the viscosity of oxygenated fuels is expressed as

$$\eta_{\mathrm{l}} = \frac{p_{\mathrm{r}} Z_{\mathrm{l}}^{\mathrm{c}}}{Z_{\mathrm{l}}} \exp\left[\left(b + \frac{c}{d + T_{\mathrm{r}}}\right) + \left(a_1 + a_2 / T_{\mathrm{r}}^2\right)\left(Z_{\mathrm{l}} - Z_{\mathrm{l}}^{\mathrm{c}}\right)\right] \tag{12}$$

where T_{r} ($=T/T_{\mathrm{c}}$), p_{r} ($=p/p_{\mathrm{c}}$) are reduced temperature and pressure, respectively, $Z_{\mathrm{l}}^{\mathrm{c}}$ is the compressibility factor at p_{r}=1. The a_1, a_2, b, c and d are parameters independent of temperature and pressure, which will be acquired by fitting to experimental data. The only variable required to be calculated in Eq. (12) is the compressibility factor, and it has been proved that the precision of the compressibility factor values has negligible influence on the accuracy of the viscosity calculation [59]. Therefore, to insure the universality and simplicity of the model, the Soave-Redlich-Kwong (SRK) equation of state [61] is chosen to estimate the compressibility factors. The critical properties and acentric factors required in SRK equation are collected from references [57, 60, 62-64].

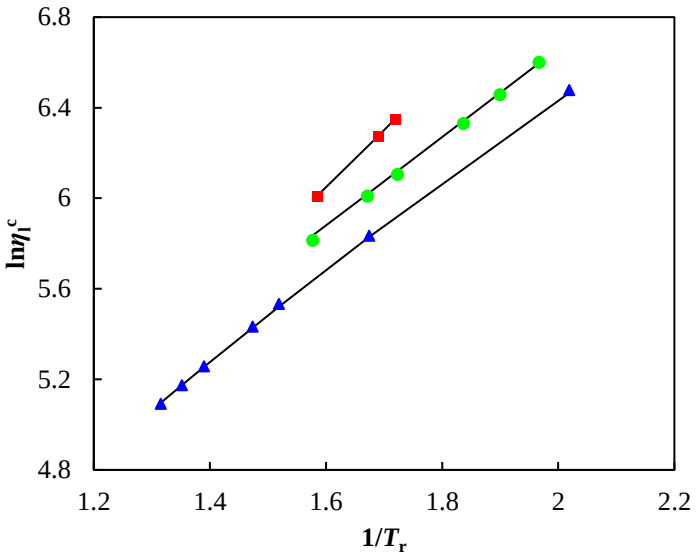

Fig. 1. Temperature dependence of viscosities at p_r=1: Experimental data: (■) MeOH [14, 15], (●) DMC [21], (▲) DMM [31]; (—) Calculated values

3. Results and discussion

3.1 Pure components

Table 1 summarizes the information of 31 oxygenated fuels used to verify the reliability of our model. A database of 1574 data points for alcohols, esters and ethers under the temperatures from 243.15 K to 413.15 K and pressures from 0.1 MPa to 200 MPa is established. The critical properties and acentric factors of these substances can be found in Table S2.

Table 1 Summary of the selected literature data

Substance[1]	CAS No.	*T*/K	*p*/MPa	Method	Uncer-tainty/%[2]	No. of data	Ref.
MeOH	67-56-1	298.15-323.15	0.1-27.05	a	1	19	14
		303.15-323.15	0.1-30	b	4	22	15
		283.15-348.15	0.1-68.8	c	4	31	16
EtOH	64-17-5	298.15-323.15	0.1-27.56	a	1	20	14
		293.15-353.15	0.1-100	c	2	23	17
		298.15-323.15	0.1-78.6	c	4	16	16
PrOH	71-23-8	298.15-323.15	0.1-27.86	a	1	20	14
		283.15-323.15	0.1-117.8	c	4	39	16
IPA	67-63-0	298.15-323.15	0.1-117.8	c	4	26	16
		303.15-343.15	0.1-100	c	2	18	18

Substance[1]	CAS No.	*T*/K	*p*/MPa	Method	Uncer-tainty/%[2]	No. of data	Ref.
PeOH	71-41-0	298.15-373.15	50-195	d	4	15	19
NPEA	584-02-1	298.15-373.15	50-195	d	4	15	19
NoOH	143-08-8	298.15-413.15	50-195	d	4	19	19
TBA	75-65-0	303.15-323.15	0.1-22.5	b	4	19	15
		298.15-348.15	0.1-68.8	c	4	13	16
VAC	108-05-4	298.15-373.15	50-195	d	4	15	19
DEA	141-28-6	303.15-373.15	0.1-19.91	a	4	40	20
DMC	616-38-6	283.15-353.15	0.1-19.52	a	4	38	21
		293.15-353.15	0.1-100	c	4	40	22
DEC	105-58-8	263.15-363.15	0.1-19.49	a	4	55	23
		283.15-353.15	0.1-100	c	4	48	22
EHE	106-30-9	312.72-353.04	0.1-15.17	b	<2.7	30	24
EOC	106-32-1	312.87-353.38	0.1-15.24	b	<2.7	30	24
MCA	110-42-9	293.15-353.15	0.1-200	e	<4	42	25
ECA	110-38-3	293.15-353.15	0.1-200	e	<4	44	25
MLA	111-82-0	302.98-353.40	0.1-15.07	b	1.5	36	26
		293.15-353.15	0.1-200	e	<4	54	27
ELA	106-33-2	302.72-353.65	0.1-15.20	b	1.5	36	26
		293.15-353.15	0.1-200	e	<4	58	27
MMY	124-10-7	303.15-353.15	0.1-100	e	2	38	28
EMY	124-06-1	293.15-353.15	0.1-100	e	2	38	28
DEE	60-29-7	243.15-373.15	0.1-19.61	a	4	70	29
DIPE	108-20-3	243.15-373.15	0.1-21.68	a	4	70	30
DBE	142-96-1	243.15-373.15	0.1-21.12	a	4	70	30
DMM	109-87-5	243.15-373.15	0.1-19.55	a	4	70	31
1GM	110-71-4	243.15-373.15	0.1-19.48	a	4	70	31
2GM	111-96-6	243.15-323.15	0.15-21.49	a	4	45	32
3GM	112-49-2	283.15-353.15	0.1-100	c	4	48	22
4GM	143-24-8	283.15-353.15	0.1-100	c	4	48	22
MEGME	109-86-4	293.15-353.15	0.1-100	c	4	42	33
MEGEE	110-80-5	293.15-353.15	0.1-100	c	4	42	33
iso-MEGPE	109-59-1	293.15-353.15	0.1-100	c	4	42	33

a: Vibrating-wire; b: Capillary c: Falling-body; d: Rolling-ball; e: Quartz resonator

[1] The full names of these substances are given in Table S2.

[2] The expanded uncertainties with 95% confidence.

For each component, the parameters in Eq. (12) are obtained by correlating the experimental data from literatures [14-33] with the Levenberg-Marquadt method, and the objective function of

this work is decided as follows

$$F_{\mathrm{ob}} = \sum_{i=1}^{N} \left(\frac{\eta_{i,\mathrm{cal}} - \eta_{i,\mathrm{exp}}}{\eta_{i,\mathrm{exp}}} \right)^2 \tag{13}$$

where F_{ob} represents the objective function, N is the number of data points, subscript cal and exp represent the calculated and experimental values. Then the parameters are reported in Table S1, and a comparison between calculated results and experimental data is also carried out and shown in Table 2 and Figs. 2-7.

Before analyzing these results and evaluating the performance of the present model, some statistical variables should be defined primarily:

$$\mathrm{Dev} = \frac{100\left(\eta_{\mathrm{cal}} - \eta_{\mathrm{exp}}\right)}{\eta_{\mathrm{exp}}} \qquad \mathrm{AARD} = \frac{1}{N}\sum_{i=1}^{N}\left|\mathrm{Dev}\right| \qquad \mathrm{MD}=\mathrm{MAX}\left|\mathrm{Dev}\right| \tag{14}$$

where Dev is relative deviation, AARD is average absolute relative deviation and MD is maximum deviation. It can be observed from Table 2, the AARD of the computed results from the experimental values are lower than 2.37%. The overall AARD of all compounds is estimated to be 1.06%, and the maximum deviation is 8.49%.

Fig. 2 compares the calculated values from our model and the experimental data of alcohols. It shows that deviations for most of the points are in the region of ±5%, and only one point for EtOH (ethanol) reach to 5.25%. For these fuels, the overall AARD of viscosities calculated from the proposed model is 1.07%, and the MD is 5.25%. Fig. 3 gives a comparison for the viscosities of PrOH at three temperatures and pressures up to 117.8 MPa. It is obvious that the performance of the present model is rather satisfactory and successfully reflects the tendency of the viscosity with pressure.

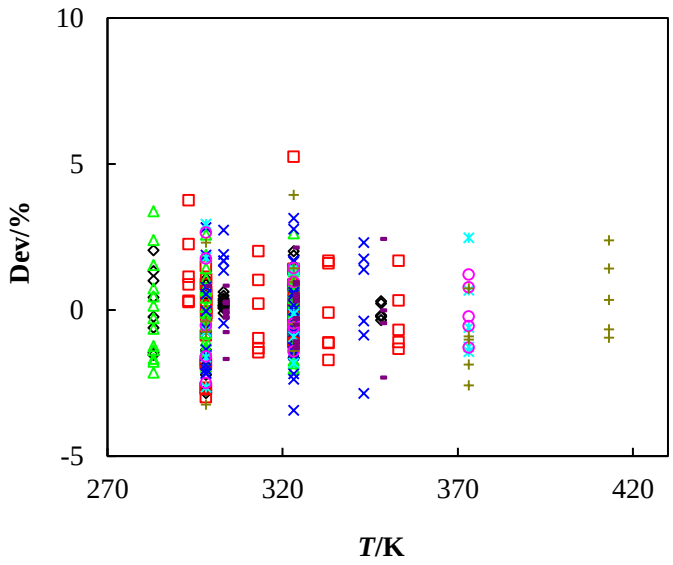

205

206 Fig. 2. Deviations of the present model from experimental data of alcohols: (◇) MeOH [14-16],

207 (□) EtOH [14, 16, 17], (△) PrOH [14, 16], (×) IPA [16, 18], (*) PeOH [19], (○) NPEA [19], (+)

208 NoOH [19], (-) TBA [15, 16].

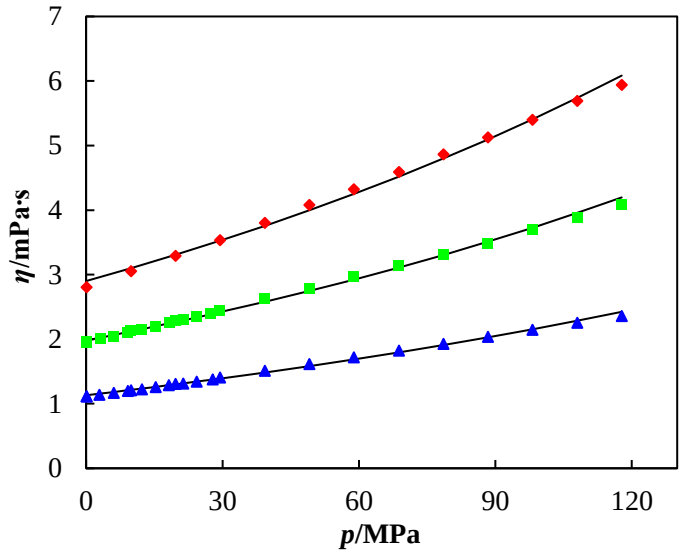

209

210 Fig. 3. Pressure dependence of the viscosities of PrOH at different temperatures: Experimental

211 data [14, 16]: (◆) 283.15 K, (■) 298.15 K, (▲) 323.15 K; (—) Calculated values.

212 Another comparison of viscosities between calculated and experimental values for 12 esters is

213 shown in Fig. 4. It indicates that the deviations of the present model for more than 98% points are

214 within ±5%, while none of the points are out of the region of ±10%. Furthermore, the AARDs of

the present model for all esters are estimated to be lower than 2.37%, which shows a good agreement with the literature data. Fig. 5 exhibits the pressure dependence of the viscosities from the present model and experiments of ECA at 4 temperatures, in which the pressures are at the range of 0.1 MPa to 200 MPa. It reveals that the present model also has good performance for the viscosities of esters.

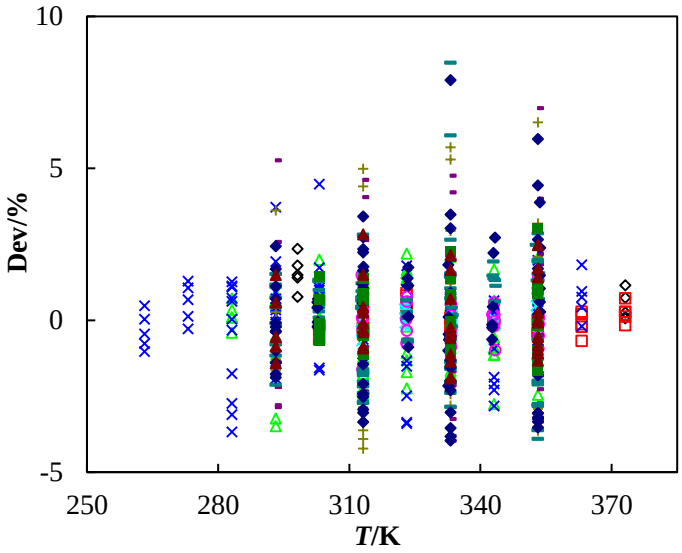

Fig. 4. Deviations of the present model from experimental data of esters: (◇) VAC [19], (□) DEA [20], (△) DMC [21, 22], (×) DEC [22, 23], (*) EHE [24], (○) EOC [24], (+) MCA [25], (-) ECA [25], (—) MLA [26, 27], (◆) ELA [26, 27], (■) MMY [28], (▲) EMY [28].

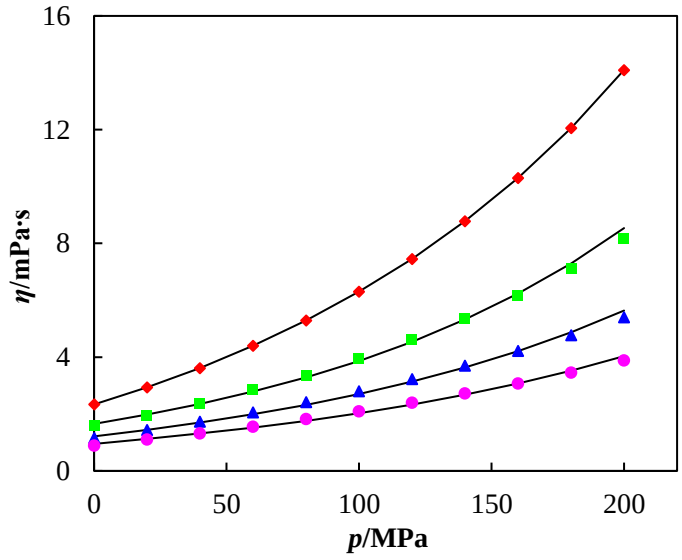

Fig. 5. Pressure dependence of the viscosities of ECA at different temperatures: Experimental data [25]: (◆) 293.15 K, (■) 313.15 K, (▲) 333.15 K, (●) 353.15 K; (—) Calculated values.

Fig. 6 illustrates the capability of the present model to correlate the viscosities of ethers. As expected, the present model is rather adequate for viscosity modeling of all these substances. The deviations of all data points are within the range of ±5%, and the overall AARD is calculated to be 0.83%. Furthermore, only deviations for 2 of 617 points go beyond the line of 4%, and the poorest agreement is observed for 4GM with the MD of 4.89%. Fig. 7 clearly shows the pressure dependence of the viscosities of MEGME at the temperatures from 293.15 K to 353.15 K, and the pressures up to 100 MPa. The present model for viscosity of ethers still has sufficient precision as before.

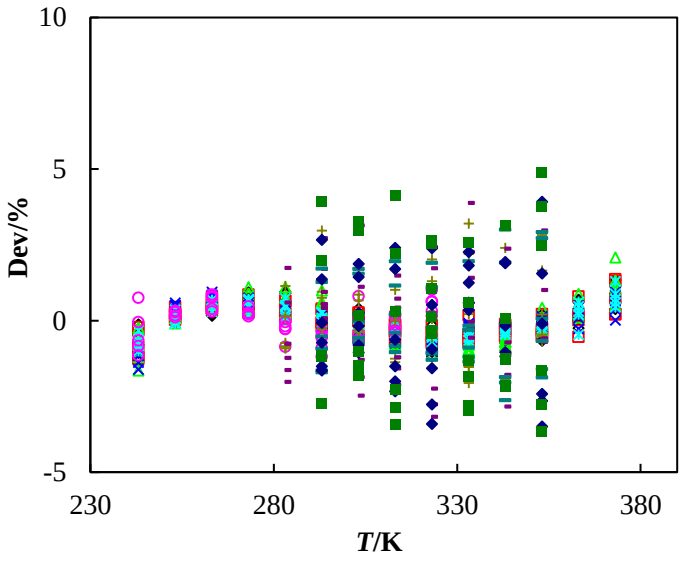

Fig. 6. Deviations of the present model from experimental data of ethers: (◇) DEE [29], (□) DIPE [30], (△) DBE [30], (×) DMM [31], (*) 1GM [31], (○) 2GM [32], (+) 3GM [22], (-) 4GM [22], (—) MEGME [33], (◆) MEGEE [33], (■) iso-MEGPE [33].

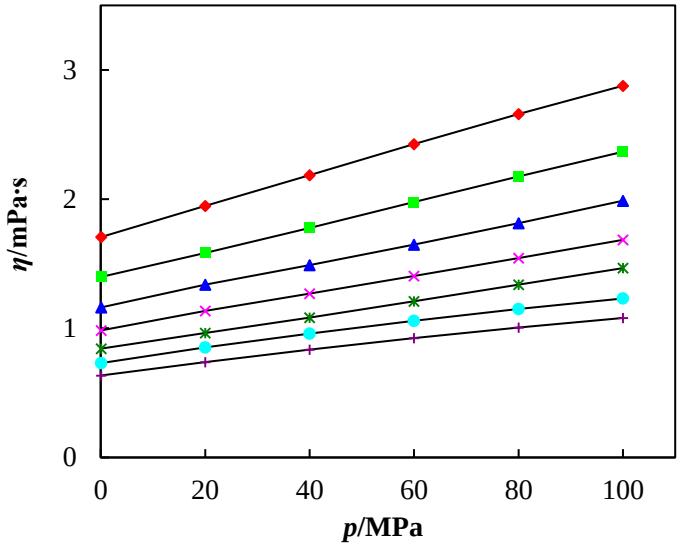

239

240 Fig. 7. Pressure dependence of the viscosities of MEGME at different temperatures: Experimental

241 data [33]: (◆) 293.15 K, (■) 303.15 K, (▲) 313.15 K, (×) 323.15 K, (*) 333.15 K, (●) 343.15 K,

242 (+) 353.15 K; (—) Calculated values.

243 As shown in Figs. 2, 4 and 6, the deviations of calculation from experiments have no apparent

244 relationship to temperature, while the increasing deviations with pressure can be observed in Figs.

245 3 and 5. Such phenomenon can be attributed to the higher uncertainties of experiments at elevated

246 pressures [25]. Nevertheless, we should mention that all of the AARDs are within the

247 experimental uncertainties and even the most of MDs. Then, from Figs. 3, 5 and 7, we can

248 conclude that the pressure effect on viscosity will become less significant with the increasing

249 temperature. The similar conclusion was drawn by Pensado et al. [65]. They consider that, at high

250 temperatures, the interactions between two molecules become weaker, which leads to a smaller

251 influence of pressure on viscosity. In addition, quite different shapes of viscosity curves with

252 pressure at the same temperature are observed in Figs. 5 and 7, which perform as a more

253 significant effect of pressure on the viscosity of ECA indicating the stronger interactions between

254 molecules than MEGME.

To further illuminate the accuracy of the proposed model for viscosity of oxygenated fuels, another widely used viscosity model named free-volume model is chosen to give a comparison. Free-volume (FV) model which has a strong physical background considers the flow energy E as two parts: the energy necessary to form the vacant vacuums $pV=pM/\rho$, and the barrier energy $E_0=\alpha_0\rho$ which the molecule must cross to diffuse [49, 50]. This assumption about flow energy is similar with the idea of our model, which is the reason why the FV model is chosen here.

From the derivation of Allal et al. [50], the FV model for the viscosity correlation is given by

$$\eta = \eta_0 + \Delta\eta \tag{15}$$

where η_0 is the viscosity of dilute gas, which can be obtained by the modified Chapman-Enskog theory proposed by Chung et al. [66]. The second term $\Delta\eta$ represents the contribution of the dense fluid, and has been expressed as

$$\Delta\eta=\rho l\frac{\sigma\rho+pM/\rho}{\sqrt{3RTM}}\exp\left[B\left(\frac{\sigma\rho+pM/\rho}{RT}\right)^{2/3}\right] \tag{16}$$

where ρ is density, M is molecule weight, σ, l and B are temperature and pressure independent parameters. The density used in Eq. (16) can also be calculated by SRK equation, and three adjustable parameters for the FV model will be obtained by fitting the data listed in Table 1.

Table 2 gives a comparison of the performance between the present model and the FV model, and the parameters of Eq. (16) can be found in Table S1. It should be noted that, in general, the present model achieves a slightly better accuracy than the FV model. The overall AARDs of our model and the FV model are 1.06% and 1.37%, and MDs are determined to be 8.49% and 14.72%, respectively. In addition, unexpectedly, the correlated results of NPEA from FV model are not satisfying, the deviations of this substance are significant (with AARD=7.83% and MD=14.72%, respectively). As to the present model, the AARD of NPEA is 1.20% and the MD is 2.66%,

277 respectively, which are much more accurate. Fig. 8 plots the viscosities of NEPA, in which the
278 geometric symbols represent the experimental data, while the solid lines and dash lines represent
279 the calculated values from the present model and the FV model, respectively. It is obvious that the
280 results from the present model are closer to experimental points than the FV model. It also should
281 be mentioned that, according to the results from FV model, there are 10 substances which have
282 MDs higher than 5%, while for the present model, such number will be reduced by half. However,
283 we should keep in mind that the FV model involves less parameters than the present model, and it
284 can be believed that if the version of FV model with more parameters should have higher accuracy
285 for the viscosities of these substances, including NPEA. It is also a pity that the present model is
286 only applicable to the liquid phase, while as mentioned in the introduction section, the FV model
287 is suitable to both gas and liquid states. So the feasible method to extend our model to gaseous and
288 even surface viscosity will be our future work.

289 Table 2 The results of the free-volume model and the present model

Substance	FV model		This work	
	AARD/%	MD/%	AARD/%	MD/%
MeOH	1.08	3.48	0.72	2.84
EtOH	0.90	3.73	1.13	5.25
PrOH	0.37	1.82	1.06	3.39
IPA	1.64	8.06	1.46	3.43
PeOH	1.13	3.37	1.45	2.95
NPEA	7.83	14.72	1.20	2.66
NoOH	3.04	6.10	1.46	3.95
TBA	2.58	9.00	0.73	2.44
VAC	1.50	3.24	0.92	2.36
DEA	1.37	3.34	0.31	0.90
DMC	1.09	4.53	1.13	3.48
DEC	1.07	3.41	1.05	4.48
EHE	0.40	1.43	0.25	0.68
EOC	0.59	1.85	0.55	1.62
MCA	1.45	4.57	2.34	6.51
ECA	1.97	5.37	2.37	7.00

MLA	1.49	5.56	1.54	8.49
ELA	1.84	8.45	1.74	7.91
MMY	1.16	3.46	0.87	3.02
EMY	1.01	3.42	0.95	2.83
DEE	0.82	4.31	0.46	1.35
DIPE	0.75	3.68	0.42	1.37
DBE	2.09	7.10	0.63	2.09
DMM	0.81	4.05	0.47	1.61
1GM	1.06	3.37	0.42	1.29
2GM	2.52	6.97	0.46	1.19
3GM	1.47	4.94	1.05	3.21
4GM	1.99	4.95	1.45	3.89
MEGME	0.80	2.31	1.24	3.02
MEGEE	1.05	3.09	1.50	3.92
iso-MEGPE	1.84	5.89	2.10	4.89
Overall values	1.37	14.72	1.06	8.49

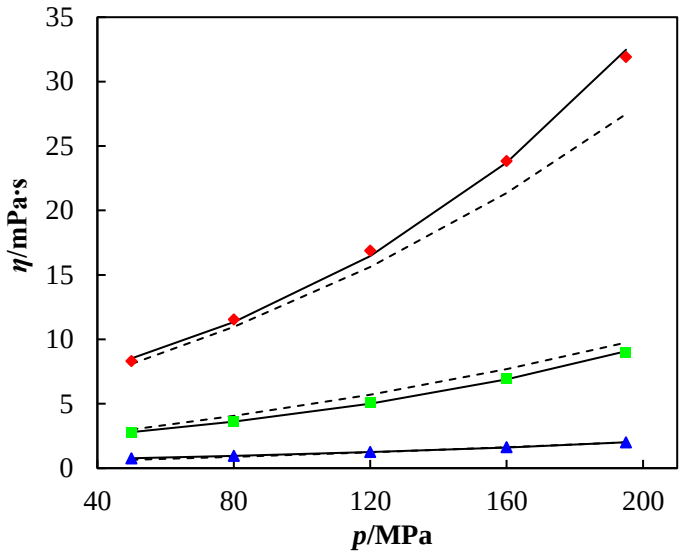

Fig. 8. Pressure dependence of the viscosities of NPEA at different temperatures: Experimental data [19]: (◆) 298.15 K, (■) 323.15 K, (▲) 373.15 K; Calculated values: (—) This work, (----) FV model.

3.2 Mixtures

Now we will preliminarily discuss the potential of our model for mixtures. Until now, numerous mixing rules have been developed for viscosities of liquid mixtures, and one of the most popular rule is the equation proposed by Grunberg and Nissan [67]. The equation is usually used to

298 calculate the viscosity of mixture at atmospheric pressure, while it is still valid for the dense fluid
299 at any constant pressure. So, in this work, for the η_l^c of binary mixture at p_r=1 in Eq (11), the
300 Grunberg-Nissan equation can be given as

301 $$\ln \eta_{l,m}^{c} = \sum_{i=1}^{2} x_i \ln \eta_{l,i}^{c} + x_1 (1 - x_1) G_{12} \quad (17)$$

302 where subscript m, 1 and 2 represent the mixture and two components, respectively. The x_1 is
303 molar fraction of component 1, and G_{12} is an interaction parameter which can be expressed as

304 $$G_{12} = \kappa / T_r \quad (18)$$

305 where κ is a mixture parameter. Then, for the parameter a in Eq. (7), the following mixing rule is
306 chosen

307 $$a_m^3 = \sum_{i=1}^{2} x_i a_i^3 \quad (19)$$

308 Because there are limited experimental viscosity data for oxygenated fuel mixtures, we used
309 one alcohol + alcohol and three alcohol + hydrocarbon mixtures to examine the validity of the
310 present model with mixing rules from Eqs. (17 to 19); the selected systems are:
311 2-Methyl-2-propanol (TBA) + methanol (MeOH) [15], ethanol (EtOH) + n-heptane (Hp) [68],
312 ethanol + toluene (Tol) [17] and 1-propanol (PrOH) + toluene [69]. Table 3 summarizes the
313 experimental data for these mixtures. The critical properties as well as acentric factors of pure
314 n-heptane and toluene obtained from reference [60] have been listed in Table S2, while the
315 parameters in Eq. (12) for them are shown in Table S1. The compressibility factors of mixtures
316 can still be calculated by SRK equation with the mixing rules introduced in reference [61].
317 However, in order to simplify the calculation process, the critical properties of mixtures will be
318 roughly treated as a linear combination of the critical properties of two pure components by the

319 molar fraction.

320 Table 3 Summary of the experimental viscosity data of mixture

Substance	*T*/K	*p*/MPa	Uncertainty/%[1]	No. of data	Ref.
TBA + MeOH	303.15-323.15	0.1-30	4	66	15
EtOH + Hp	293.15-353.15	0.1-100	4	161	68
EtOH + Tol	293.15-353.15	0.1-100	2	162	17
PrOH + Tol	293.15-353.15	0.1-100	4	168	69

321 [1]The expanded uncertainties with 95% confidence.

322 Before correlating the mixture parameter in Eq. (18), the predictive ability of the proposed
323 mixing rules with the κ in Eq. (18) equal 0 was tested. In addition, for a comparison purpose, the
324 mixing rules for the FV model without any extra parameters are also used to predict the viscosities
325 of these mixtures, and the parameters in Eq. (16) for pure n-heptane and toluene can also be found
326 in Table S1. There are many mixing rules have been developed for the FV model, while in this
327 work, the simple and widely used mixing rules proposed by Comuñas et al. [70] are chosen, which
328 are

329 $$\ln \eta_{0,\mathrm{m}} = \sum_{i=1}^{2} x_i \ln \eta_{0,i} \tag{20}$$

330 $$\sigma_{\mathrm{m}} = \sum_{i=1}^{2}\sum_{j=1}^{2} x_i x_j \sigma_{ij}, \qquad \sigma_{ij} = \left(\sigma_i \sigma_j\right)^{1/2} \tag{21}$$

331 $$l_{\mathrm{m}} = \sum_{i=1}^{2} x_i l_i \tag{22}$$

332 $$1/B_{\mathrm{m}} = \sum_{i=1}^{2} x_i / B_i \tag{23}$$

333 Then the comparisons between the calculations and experiments are shown in Fig. 9, where the
334 dash line is the ideal results without any deviations. It seems a pity that both of models fail to
335 predict the viscosities of these mixtures, and the only acceptable results are from EtOH + Hp
336 calculated by the FV model with the AAD of 7.13% and MD of 12.82%, respectively. In particular,

most of the calculated points are overestimated in Fig. 9, while the results of TBA + MeOH from the present model tend to be underestimated, which arises from the special interactions between the two molecules of TBA + MeOH.

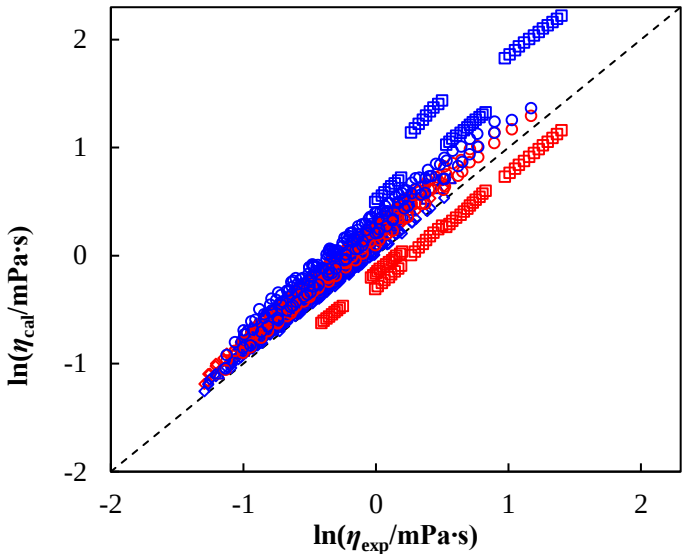

Fig. 9. Comparisons between the experiments and the calculations by the present model (red) and the FV model (blue) without mixture parameters: (□) TBA + MeOH, (◇) EtOH + Hp, (Δ) EtOH + Tol, (○) PrOH + Tol, (---) Dev=0.

As it is failed to predict the mixture viscosities using the mixing rules without any extra parameters, the κ in Eq. (18) should be necessary for improving the calculation accuracy. As for the FV model, there is no doubt that using the different mixing rules can significant affect the final results, hence the performance of the FV model for the selected mixtures may be improved if more different mixing rules are attempted. Nevertheless, in this work, in order to be consistent with the present model, another mixing rule proposed by Cain et al. [71] is adopted, which modifies the Eq. (21) by adding a mixture parameter, then gives

$$\sigma_{\mathrm{m}}=\sum_{i=1}^{2}\sum_{j=1}^{2}x_i x_j \sigma_{ij}, \qquad \sigma_{ij}=\left(\sigma_i \sigma_j\right)^{1/2}\left(1-k_{ij}\right) \tag{24}$$

here $k_{11}=k_{22}=0$ and $k_{12}=k_{21}$. Then the mixture parameters κ as well as k_{12} are correlated by fitting

353 the experimental data, which are finally given in Table 4.

354 Table 4 and Fig. 10 give the results of two models for the selected mixtures, and show a
355 remarkable improvement compared with the results without mixture parameters. The overall
356 AARD of our model for four mixtures is 1.55%, and the MD is lower than 6.43%, which are
357 comparable with the FV model. However, the performance of the FV model for TBA + MeOH is
358 still unsatisfactory, so the mixing rules which are more applicable for this kind of mixture should
359 be further discussed. It is also remarkable that the κ for TBA + MeOH shows a positive value,
360 while three negative values can be got for the alcohol + hydrocarbon mixtures, which are just
361 consistent to the underestimate of TBA + MeOH and the overestimate of the other three mixtures
362 when the κ isn't adopted in the mixing rules. Such difference may be attributed to the different
363 performance of these mixtures viscosities, which is mainly caused by the influence of hydrogen
364 bonds between molecules. Fig. 11 compares our calculated values and experimental data for
365 viscosity of EtOH (1) + Tol (2), where the dash lines represent the ideal values which is defined by
366 $\eta_m=x_1\eta_1+x_2\eta_2$. Obviously, the computed results have a quite agreement with experimental values at
367 all compositions. Furthermore, comparing the solid and dash curves, the negative deviations of
368 mixture viscosities from ideal values are observed, which arises from the disruption of the ordered
369 molecular structure and the weakening or breaking of the self-association between ethanol
370 molecules [17]. Then, the comparisons of viscosities between TBA + MeOH and EtOH + Hp at
371 T=323.15 K and p=0.1 MPa are implemented in Fig. 12. It should be declared that as the
372 experimental temperatures of TBA + MeOH and EtOH + Hp are totally different, while in order to
373 discuss the two mixtures at the same condition, the viscosities of EtOH + Hp at T=323.15 K and
374 p=0.1 MPa are just given by calculations. Then from Fig. 12, the negative departures of EtOH +

Hp viscosities from ideality are acquired, which lead to the negative values of κ in Eq. (18). However, the viscosities of TBA + MeOH have positive deviations from ideal values, which may result from the hydrogen bond effect between two molecules [72] and result in a positive value of κ.

Table 4 Performance of the mixing rules with mixture parameters

Substance	FV model			This work		
	k_{12}	AARD/%	MD/%	κ	AARD/%	MD/%
TBA + MeOH	0.2663	27.60	44.16	0.6611	3.38	6.18
EtOH + Hp	0.05488	2.16	6.07	-0.5331	1.22	4.11
EtOH + Tol	0.1692	2.26	7.35	-0.3867	0.97	3.76
PrOH + Tol	0.2039	2.70	9.34	-0.6317	1.71	6.43
Overall values		5.37	44.16		1.55	6.43

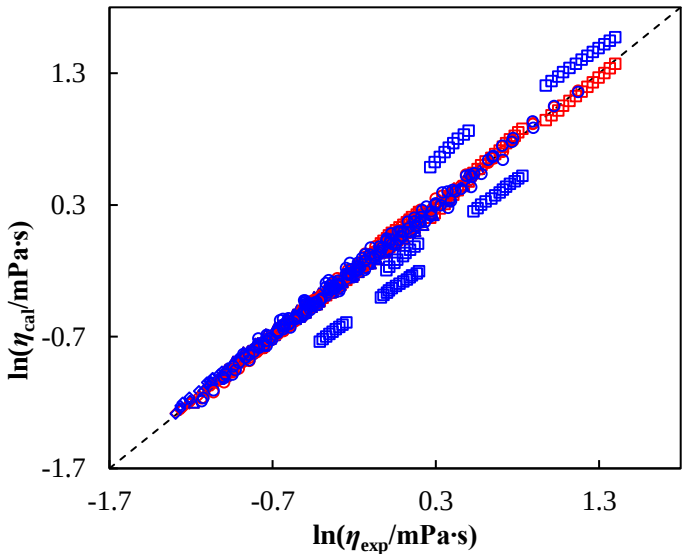

Fig. 10. Comparisons between the experiments and the calculations by the present model (red) and the FV model (blue) with mixture parameters: (□) TBA + MeOH, (◇) EtOH + Hp, (Δ) EtOH + Tol, (○) PrOH + Tol, (---) Dev=0.

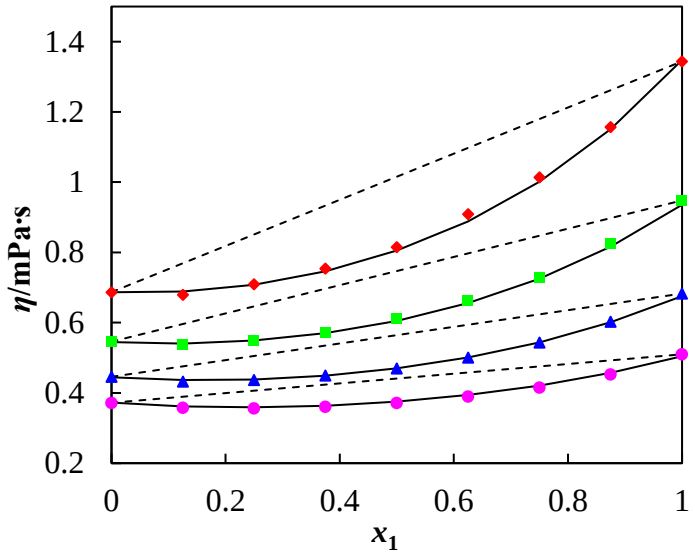

384

385 Fig. 11. Molar fraction (x_1) dependence of the viscosities of EtOH (1) + Tol (2) at different

386 temperatures and p=20 MPa: Experimental data [17]: (◆) 293.15 K, (■) 313.15 K, (▲) 333.15 K,

387 (●) 353.15 K; (—) Calculated values; (---) Ideal curves.

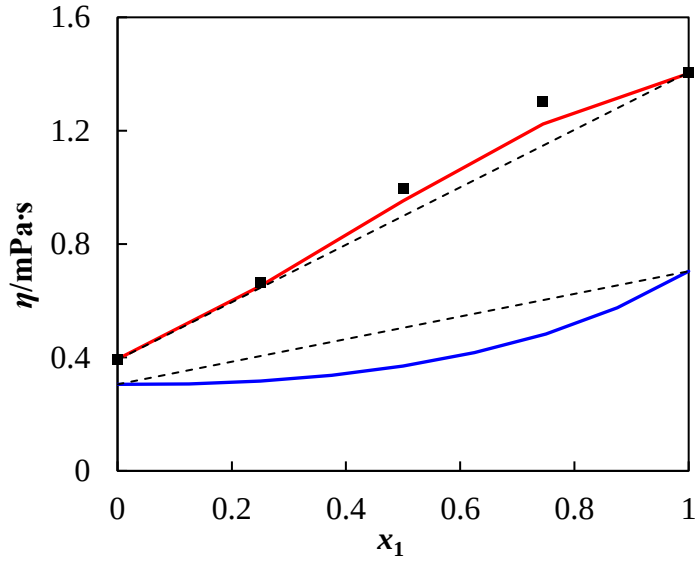

388

389 Fig. 12. Molar fraction (x_1) dependence of the viscosities of 4 mixtures at T=323.15 K and p=0.1

390 MPa: Experimental data [15]: (■) TBA (1) + MeOH (2); Calculated values: (—) TBA (1) + MeOH

391 (2), (—) EtOH (1) + Hp (2); (---) Ideal curves.

392 **4. Conclusion**

393 Based on Eyring's absolute rate theory, we present a simple and accurate viscosity model for

394 oxygenated-hydrocarbons relevant to fuels in a wide range of temperature and pressure. The core
395 concept of our model is to treat the flow energy as a combination of activation energy and the
396 vacancy-formation energy. And the developments of the present model comparing with others
397 based on Eyring's theory are concluded on two points: without considering the specific form of
398 activation energy and proposing a reference state to eliminate the activation energy term. The only
399 variable required in this model is the compressibility factor which can be calculated by a cubic
400 equation of state such as SRK equation.

401 A database compiled viscosities of 31 oxygenated fuel components at temperatures from 243.15
402 K to 413.15 K and pressures from 0.1 MPa to 200 MPa was built. The present model coupled with
403 SRK equation was tested by these literature data, and the overall AARD was decided to be 1.06%,
404 while the MD was 8.49%. Furthermore, the present model with 5 parameters was compared with
405 the 3-parameters free-volume model, and the former one delivered better accuracy than the latter
406 as well as better correlated to the viscosities of 3-pentanol (NPEA) reported by Ref. [19].

407 At last, the feasibility of the present model extending to mixtures was verified by calculating the
408 viscosities of 4 binary mixtures containing oxygenated fuels, and a quite satisfying performance
409 can be obtained from the results.

410 **Acknowledgement**

411 The authors gratefully acknowledge the supports provided by the National Science Fund for
412 Distinguished Young Scholars of China [No. 51525604], the Foundation for Innovative Research
413 Groups of the National Natural Science Foundation of China [No.51721004], the National Basic
414 Research Program of China [No. 2015CB251502] and 111 Project [No. B16038].

415 **Appendix A. Supplementary data**

The parameters of the present model and the FV model are given in Table S1. The details of selected oxygenated fuels in this work are listed in Table S2.

References

[1] Colonna P, Casati E, Trapp C, Mathijssen T, Larjola J, Turunen-Saaresti T, Uusitalo A. Organic Rankine cycle power systems: from the concept to current technology, applications, and an outlook to the future. J. Eng. Gas. Turbines Power 2015;137:100801/1−19.

[2] Liu X, Pan P, Yang F, He M. Solubilities and diffusivities of R227ea, R236fa and R245fa in 1-hexyl-3-methylimidazolium bis (trifluoromethylsulfonyl) imide. J. Chem. Thermodyn. 2018;123:158−164.

[3] Agrafiotis C, Roeb M, Sattler C. A review on solar thermal syngas production via redox pair-based water/carbon dioxide splitting thermochemical cycles. Renew. Sust. Energ. Rev. 2015;42:254−285.

[4] Jin H, Zhao X, Guo L, Zhu C, Cao C, Wu Z. Experimental investigation on methanation reaction based on coal gasification in supercritical water. Int. J. Hydrog. Energy 2017;42:4636−4641.

[5] Liu X, Liu S, Bai L, Wang T, He M. Absorption and separation of CO_2/C_3H_8 and C_3H_6/C_3H_8 by ionic liquid: Effect of molar volume. J. Nat. Gas Sci. Eng. 2018. https://doi.org/10.1016/j.jngse.2018.07.018

[6] Liu X, Pan P, He M. Vapor-liquid equilibrium and diffusion coefficients of R32+[HMIM][FEP], R152a+[HMIM][FEP] and R161+[HMIM][FEP]. J. Mol. Liq. 2018;253:28−35.

[7] Mehta BH, Mandalia HV, Mistry AB. A review on effect of oxygenated fuel additive on the

438 performance and emission characteristics of diesel engine. National conference on recent trends in
439 engineering & technology; 2011. p. 13−14.
440 [8] Song J, Cheenkachorn K, Wang J, Perez J, Boehman AL. Effect of oxygenated fuel on
441 combustion and emissions in a light-duty turbo diesel engine. Energy Fuels 2002;16:294−301.
442 [9] Aissa MA, Ivanis GR, Radovic IR, Kijevčanin MJ. Experimental investigation and modeling
443 of thermophysical properties of pure methyl and ethyl esters at high pressures. Energy Fuels
444 2017;31:7110−7122.
445 [10] Su C, Zhu C, Yang F, Ye Z, Liu X, He M. Isobaric Molar Heat Capacity of Ethyl Octanoate
446 and Ethyl Decanoate at Pressures up to 24 MPa. J. Chem. Eng. Data 2018;63:2252−2256.
447 [11] He M, Wang C, Chen J, Liu X, Xin N, Zhang Y. Measurement of critical properties for binary
448 and ternary mixtures containing potential gasoline additive diethyl carbonate (DEC). Fluid Phase
449 Equilib. 2018;471:17−23.
450 [12] Dzida M, Jężak S, Sumara J, Żarska M, Góralski P. High-pressure physicochemical
451 properties of ethyl caprylate and ethyl caprate. J. Chem. Eng. Data 2013;58:1955−1962.
452 [13] Wu Z, Zhu Z, Huang Z. An experimental study on the spray structure of oxygenated fuel
453 using laser-based visualization and particle image velocimetry. Fuel 2006;85:1458−1464.
454 [14] Assael MJ, Polimatidou SK. Measurements of the viscosity of alcohols in the temperature
455 range 290–340 K at pressures up to 30 MPa. Int. J. Thermophys. 1994;15:95−107.
456 [15] Matsuo S, Makita T. Viscosity of methanol and 2-methyl-2-propanol mixtures under high
457 pressures. Int. J. Thermophys. 1991;12:459−468.
458 [16] Tanaka Y, Matsuda Y, Fujiwara H, Kubota H, Makita T. Viscosity of (water+ alcohol)
459 mixtures under high pressure. Int. J. Thermophys. 1987;8:147−163.

460 [17] Zeberg-Mikkelsen CK, Baylaucq A, Watson G, Boned C. High-pressure viscosity
461 measurements for the ethanol+ toluene binary system. Int. J. Thermophys. 2005;26:1289−1302.
462 [18] Moha-Ouchane M, Boned C, Allal A, Benseddik M. Viscosity and excess volume at high
463 pressures in associative binaries. Int. J. Thermophys. 1998;19:161−189.
464 [19] Sülzner U, Luft G. Effect of hydrogen bonding on the viscosity of alcohols at high pressures.
465 Int. J. Thermophys. 1997;8:1355−1367.
466 [20] Meng X, Zheng P, Wu J, Liu Z. Density and viscosity measurements of diethyl adipate from
467 (303 to 373) K and up to 20 MPa. J. Chem. Eng. Data 2008;53:1474−1478.
468 [21] Meng X, Zheng P, Wu J, Liu Z. Viscosity and density measurements of dimethyl carbonate. J.
469 Eng. Thermophys. (China) 2009;30:26−30.
470 [22] Comuñas M J P, Baylaucq A, Boned C, Fernández J. High-pressure measurements of the
471 viscosity and density of two polyethers and two dialkyl carbonates. Int. J. Thermophys.
472 2001;22:749−768.
473 [23] Meng X, Zheng P, Wu J. Measurements of viscosity and density of diethyl carbonate. J.
474 Chem. Ind. Eng. (China) 2008;59:2695−2700.
475 [24] Liu X, Lai T, Guo X, He M, Dong W, Shang T, Yang W. Densities and viscosities of ethyl
476 heptanoate and ethyl octanoate at temperatures from 303 to 353 K and at pressures up to 15 MPa.
477 J. Chem. Eng. Data 2017;62:2454−2460.
478 [25] Habrioux M, Bazile JP, Galliero G, Daridon JL. Viscosities of fatty acid methyl and ethyl
479 esters under high pressure: methyl caprate and ethyl caprate. J. Chem. Eng. Data
480 2015;60:902−908.
481 [26] He M, Lai T, Liu X. Measurement and correlation of viscosities and densities of methyl

dodecanoate and ethyl dodecanoate at elevated pressures. Thermochim. Acta 2018;663:85−92.

[27] Habrioux M, Nasri D, Daridon JL. Measurement of speed of sound, density compressibility and viscosity in liquid Methyl Laurate and Ethyl Laurate up to 200 MPa by using acoustic wave sensors. J. Chem. Thermodyn. 2018;120:1−12.

[28] Habrioux M, Bazile JP, Galliero G, Daridon JL. Viscosities of fatty acid methyl and ethyl esters under high pressure: methyl myristate and ethyl myristate. J. Chem. Eng. Data 2016;61:398−403.

[29] Meng X, Zheng P, Wu J, Liu Z. Density and viscosity measurements of diethyl ether from 243 to 373 K and up to 20 MPa. Fluid Phase Equilib. 2008;271:1−5.

[30] Meng X, Wu J, Liu Z. Viscosity and density measurements of diisopropyl ether and dibutyl ether at different temperatures and pressures. J. Chem. Eng. Data 2009;54:2353−2358.

[31] Zheng P, Meng X, Wu J, Liu Z. Density and viscosity measurements of dimethoxymethane and 1,2-dimethoxyethane from 243 K to 373 K up to 20 MPa. Int. J. Thermophys. 2008;29:1244−1256.

[32] Meng X. Density and viscosity measurements of diethylene glycol dimethyl ether. J. Eng. Thermophys. (China) 2010; 31:1465−1469.

[33] Reghem P, Baylaucq A, Comuñas MJP, Fernándezb J, Boneda C. Influence of the molecular structure on the viscosity of some alkoxyethanols. Fluid Phase Equilib. 2005;236:229−236.

[34] Sastri SRS, Rao KK. A new group contribution method for predicting viscosity of organic liquids. Chem. Eng. J. 1992;50: 9−25.

[35] Yinghua L, Peisheng M, Ping L. Estimation of liquid viscosity of pure compounds at different temperatures by a corresponding-states group-contribution method. Fluid Phase Equilib.

2002;198: 123−130.

[36] Ivanciuc O, Ivanciuc T, Filip PA, Cabrol-Bass D. Estimation of the liquid viscosity of organic compounds with a quantitative structure-property model. J. Chem. Inf. Comput. Sci. 1999;39:515−524.

[37] Katritzky AR, Chen K, Wang Y, Karelson M, Lucic B, Trinajstic N, Suzuki T, SchuÈ uÈ rmann G. Prediction of liquid viscosity for organic compounds by a quantitative structure-property relationship. J. Phys. Org. Chem. 2000;13:80−86.

[38] Jossi JA, Stiel LI, Thodos G. The viscosity of pure substances in the dense gaseous and liquid phases. AIChE J. 1962;8:59−63.

[39] Yarranton HW, Satyro MA. Expanded fluid-based viscosity correlation for hydrocarbons. Ind. Eng. Chem. Res. 2009;48:3640−3648.

[40] Satyro MA, Yarranton HW. Expanded fluid-based viscosity correlation for hydrocarbons using an equation of state. Fluid Phase Equilib. 2010;298:1−11.

[41] Assael MJ, Dymond JH, Papadaki M, Patterson PM. Correlation and prediction of dense fluid transport coefficients. I. n-alkanes. Int. J. Thermophys. 1992;13:269−281.

[42] Assael MJ, Dymond JH, Polimatidou SK. Correlation and prediction of dense fluid transport coefficients. VI. n-alcohols. Int. J. Thermophys. 1994;15:189−201.

[43] Assael MJ, Dymond JH, Patterson PM. Correlation and prediction of dense fluid transport coefficients. V. Aromatic hydrocarbons. Int. J. Thermophys. 1992;13:895−905.

[44] Assael MJ, Dymond JH, Polimatidou SK. Correlation and prediction of dense fluid transport coefficients. VII. Refrigerants. Int. J. Thermophys. 1995;16:761−772.

[45] Quiñones-Cisneros SE, Zéberg-Mikkelsen CK, Stenby EH. The friction theory (f-theory) for

526 viscosity modeling. Fluid Phase Equilib. 2000;169:249−276.

527 [46] Zéberg-Mikkelsen CK, Quiñones-Cisneros SE, Stenby EH. Viscosity modeling of associating

528 fluids based on the friction theory: pure alcohols. Fluid Phase Equilib. 2002;194:1191−1203.

529 [47] Quiñones-Cisneros SE, Zéberg-Mikkelsen CK, Stenby EH. One parameter friction theory

530 models for viscosity. Fluid Phase Equilib. 2001;178:1−16.

531 [48] Quiñones-Cisneros SE, Deiters UK. Generalization of the friction theory for viscosity

532 modeling. J. Phys. Chem. B 2006;110:12820−12834.

533 [49] Allal A, Moha-Ouchane M, Boned C. A new free volume model for dynamic viscosity and

534 density of dense fluids versus pressure and temperature. Phys. Chem. Liq. 2001;39:1−30.

535 [50] Allal A, Boned C, Baylaucq A. Free-volume viscosity model for fluids in the dense and

536 gaseous states. Phys. Rev. E 2001;64:011203/1−10.

537 [51] He M, Qi X, Liu X, Su C, Lv N. Estimating the viscosity of pure refrigerants and their

538 mixtures by free-volume theory. Int. J. Refrig. 2015;54:55−66.

539 [52] Kincaid JF, Eyring H, Stearn AE. The Theory of Absolute Reaction Rates and its Application

540 to Viscosity and Diffusion in the Liquid State. Chem. Rev., 1941;28:301−365.

541 [53] Xuan A, Wu Y, Peng C, Ma P. Correlation of the viscosity of pure liquids at high pressures

542 based on an equation of state. Fluid phase equilib. 2006;240:15−21.

543 [54] Martins RJ, Cardoso MJEM, Barcia OE. A new model for calculating the viscosity of pure

544 liquids at high pressures. Ind. Eng. Chem. Res. 2003;42:3824−3830.

545 [55] Lei Q, Hou Y, Lin S. Correlation of viscosities of pure liquids in a wide temperature range.

546 Fluid Phase Equilib. 1997;140:221−231.

547 [56] Macías-Salinas R, García-Sánchez F, Hernández-Garduza O. Viscosity model for pure liquids

548 based on Eyring theory and cubic EOS. AIChE J. 2003;49:799−804.
549 [57] Meng X, Wu J. Viscosity modeling of some oxygenated fuels. Fuel 2013;107:309−314.
550 [58] Liu GJ, Hu Y. Viscosity and Internal Pressure for Liquids. Acta Chim. Sin. 1991;49:649−655.
551 [59] He M, Zhu C, Liu X. Estimating the viscosity of ionic liquid at high pressure using Eyring's
552 absolute rate theory. Fluid Phase Equilib. 2018;458:170−176.
553 [60] Poling BE, Prausnitz JM, John POC. The properties of gases and liquids. 5th ed. New York:
554 Mcgraw-hill; 2001.
555 [61] Soave G. Equilibrium constants from a modified Redlich-Kwong equation of state. Chem.
556 Eng. Sci. 1972;27:1197−1203.
557 [62] Yaws CL. Thermophysical properties of chemicals and hydrocarbons. 2nd ed. New York:
558 William Andrew; 2009.
559 [63] Shimoyama Y, Iwai Y, Jin BS, Hirayama T, Arai Y. Measurement and correlation of
560 vapor-liquid equilibria for methanol+ methyl laurate and methanol+ methyl myristate systems
561 near critical temperature of methanol. Fluid Phase Equilib. 2007;257:217−222.
562 [64] Shimoyama Y, Iwai Y, Abeta T, Arai Y. Measurement and correlation of vapor-liquid
563 equilibria for ethanol+ ethyl laurate and ethanol+ ethyl myristate systems near critical temperature
564 of ethanol. Fluid Phase Equilib. 2008;264:228−234.
565 [65] Pensado AS, Comuñas MJP, Lugo L, Fernández J. High-pressure characterization of dynamic
566 viscosity and derived properties for squalane and two pentaerythritol ester lubricants:
567 pentaerythritol tetra-2-ethylhexanoate and pentaerythritol tetranonanoate. Ind. Eng. Chem. Res.,
568 2006;45:2394−2404.
569 [66] Chung TH, Ajlan M, Lee LL, Starling KE. Generalized multiparameter correlation for

570 nonpolar and polar fluid transport properties. Ind. Eng. Chem. Res. 1988;27:671−679.

571 [67] Grunberg L, Nissan AH. Mixture law for viscosity. Nature 1949;164:799−800.

572 [68] Zéberg-Mikkelsen CK, Watson G, Baylaucq A, Galliéro G, Boned C. Comparative
573 experimental and modeling studies of the viscosity behavior of ethanol+ C7 hydrocarbon mixtures
574 versus pressure and temperature. Fluid Phase Equilib. 2006;245:6−19.

575 [69] Baylaucq A, Watson G, Zéberg-Mikkelsen C, Bazile JP, Boned C. Dynamic viscosity of the
576 binary system 1-propanol+ toluene as a function of temperature and pressure. J. Chem. Eng. Data
577 2009;54:2715−2721.

578 [70] Comuñas MJP, Baylaucq A, Boned C, Fernández J. Dynamic viscosity for HFC-134a+
579 polyether mixtures up to 373.15 K and 140 MPa at low polyether concentration. Measurements
580 and modeling. Ind. Eng. Chem. Res. 2004;43:804−814.

581 [71] Cain N, Roberts G, Kiserow D, Carbonell R. Modeling the thermodynamic and transport
582 properties of decahydronaphthalene/propane mixtures: Phase equilibria, density, and viscosity.
583 Fluid Phase Equilib. 2011;305:25−33.

584 [72] Wang CC, Chen HW, Tu CH. Densities, viscosities, and refractive indices for binary and
585 ternary mixtures of ethanol, 2-methylpropan-2-ol, and 2, 2, 4-trimethylpentane. J. Chem. Eng.
586 Data 2005;50:1687−1693.